LIGHT CURVES APPLICATION TO SPACE DEBRIS CHARACTERIZATION AND CLASSIFICATION

Jiří Šilha[(1)], Matej Zigo[(1)], Tomáš Hrobár[(1)], Peter Jevčák[(1)], Martina Verešvárska[(1,2)]

[(1)] Faculty of Mathematics, Physics and Informatics, Comenius University, Mlynska dolina, Bratislava, Slovakia, Email:jiri.silha@fmph.uniba.sk, matej.zigo@fmph.uniba.sk, hrobar2@uniba.sk, peter.jevcak@fmph.uniba.sk
[(2)] University of Southampton, University Road, Southampton SO17 1BJ, Email: mv1n17@soton.ac.uk

ABSTRACT

Photometry is commonly used method in astronomy to extract physical and dynamical (rotation) properties of space objects, such as space debris and asteroids. Once the light curve is folded into the apparent rotation period, the complexity of the signal can be much better analyzed, and amplitude of the signal can be extracted. Light curve acquired over larger arcs of phase angles provides additional physical properties about the object such as absolute magnitude and slope factor, both related to the size, surface properties and albedo of the object. Databases of space debris light curves such as Mini-MegaTORTORA (MMT) catalogue and Comenius University's Space Debris Light Curve Database (SDLCD) allow to search for cross-correlations between different measured parameters and given population types with main objective to characterize and/or classify/identify these objects.

1 INTRODUCTION

Basis of the astronomical photometry of space objects such as space debris and asteroids, is to collect the sunlight reflected from the surface of the object toward observer or sensor. Brightness of the object varies according to the range and mutual geometry defined trough the phase angle α, an angle between the observer, object and sun. Rotation of the object and the mutual geometry between the rotation axis and sensor's line of sight forms periodical change in incoming signal intensity. How bright the object is in specific moment is strongly linked to its range, cross-section C, its reflectance properties (geometric ρ_v and bond albedo ρ_b) and surface additional properties such as roughness or porosity for natural objects.

Classification of space objects can be performed by comparing several different measured quantities towards each other. In general, we can focus on standard and absolute magnitude H, slope factor parameter(s) G and/or G_1 and G_2, amplitude A and complexity X of the incoming signal.

Characterization of space objects is linked to extracting specific physical parameters. It is possible to describe a three-dimensional object with physical quantities such as shape, size, surface composition/properties, and mass or density. Size and shape can be described via dimensions ratio (ratio between major and minor axis of the object) and object's complexity (e.g. two solar panels and bus present on box-wing satellites resulting to four distinguishable peaks in light curve). This information can be extracted to certain level from light curve photometry [1]. Surface composition/properties is defined by its color, reflectivity/albedo and roughness, porosity, etc. These parameters can be extracted by using spectroscopy, BVRI photometry [2] and light curve photometry [3]. Once mean cross section is known, by applying area-to-mass ratio which can be extracted from astrodynamics analysis [4], the mass of object and consequently density of the object can be extracted.

2 PHOTOMETRY AND LIGHT CURVES

Within this work we will be focusing on the classification and characterization of objects for which one is able to extract apparent (synodic) rotation period and construct rotation phase. This is possible only for objects which have enough fast own rotation that it is captured at least several times during one data series acquisition.

2.1 Data reduction

Hereafter is discussed the photometric reduction performed at Faculty of Mathematics, Physics and Informatics, Comenius University [5]. Example of light curve obtained for rotating upper stage Titan 3C Transtage R/B (74039C) can be seen in Fig. 1.

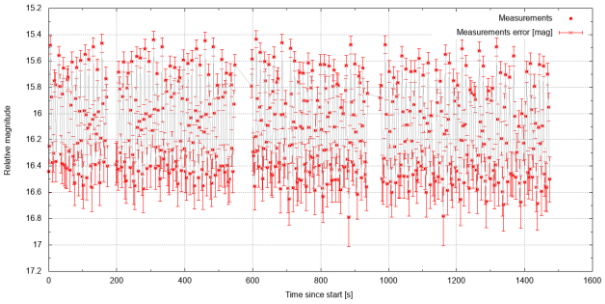

Figure 1. Light curve of object Titan 3C Transtage R/B (74039C). Photometric measurements acquired by AGO 70cm telescope during night 15th of October 2017.

Once the photometric data are acquired, and the light curve is constructed, we extract the synodic period P present in the signal. For period extraction we use frequency analysis based on algorithms such as Fast Fourier Transform (FFT), Lomb-Scargle [6] and Phase Dispersion Minimization (PDM) published in [7]. The initial analysis is performed by using FFT or Lomb-Scargle to identify the candidate frequencies present in the time series. Then, the PDM is used to reconstruct the rotation phase for the instrumental/standard magnitude, m_i as a function of phase Φ, and to obtain the measured period P. Once P is found, the rotation phase is constructed.

2.2 Rotation phase parameters

To mathematically represent the data, we fit the rotation phase with Fourier series, practice commonly used in asteroid domain [8]:

$$\Phi = a_0 + \sum_{j=1}^{n} \left(a_n cos(j\ m_i\ 2\pi) + b_n sin(j\ m_i\ 2\pi)\right) \quad (1)$$

where n is the number of harmonics and a_0, a_j, b_j, are coefficients to be found.

Once the Fit series is obtained, the signal's amplitude A can be calculated by searching the maximum and minimum of the function. The complexity of the signal X can be determined by using derivative of the obtained Fourier function. In this case we look for number of extrema, maxima or minima, in the signal. In case we have cylindrical object like upper stages, it is expected to have complexity of rotation phase signal X = 2, while for box-wing satellites it is expected to have X = 4.

Example of fitted series can be seen in Fig. 2. Plotted is rotation phase of object Titan 3C Transtage R/B (74039C) with folded 486 measurement points (blue points) and Fourier series, 8th degree marked as red line. For this rotation curve was estimated apparent rotation period of P = 25.2 s, amplitude A = 1.2 mag and complexity X = 3.

For the full light curve reduction process, please, refer to [5].

2.3 Phase function parameters

Additional quantities can be extracted once the object is observed under wide range of phase angles. Brightness dependency on phase angle is called phase function. Commonly used phase functions are lunar phase, diffuse sphere and specular sphere. Examples of these functions can be shown in Fig. 3.

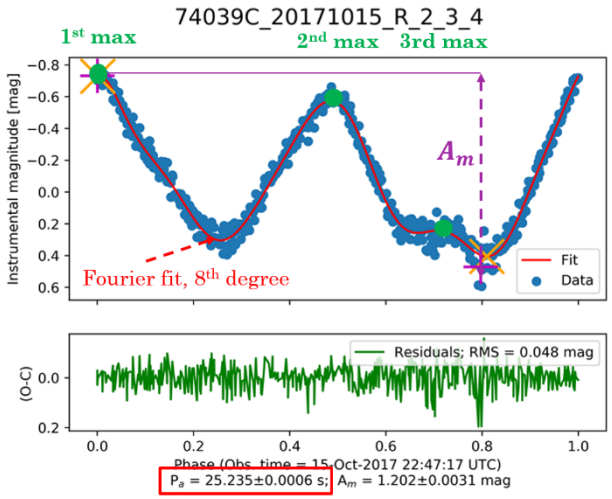

Figure 2. Light curve's rotation phase diagram of object Titan 3C Transtage R/B (74039C). Photometric measurements acquired by AGO 70cm telescope during night 15th of October 2017.

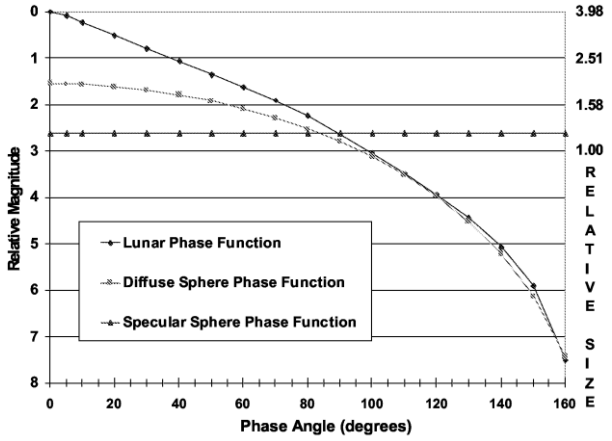

Figure 3. The commonly used phase functions. Taken from [3].

By following work [9] good approximation for phase function is mixture "diffuse-specular" model which contains phase function for diffuse sphere $F_1(\alpha)$ (Eq. 2) but also for specular sphere $F_2(\alpha)$ (Eq. 3):

$$F_1(\alpha) = \frac{2}{3\pi^2}[(\pi - \alpha)cos\alpha + sin\alpha] \quad (2)$$

$$F_2(\alpha) = \frac{1}{4\pi} \quad (3)$$

There is a high interest in minor planet community to investigate surface properties of asteroids focusing on porosity, roughness, particle size, complex refractive index, etc. It has been observed over the years that the asteroid population phase function usually contains two different components, linear dependency for higher phase angles (α > 5°) and the so-called opposition

effect, which is sudden brightening of the object due to the shadow hiding and coherent-backscatter [10], which typical for small phase angles (α > 0-5°). Phase function is usually unique for given asteroid population and is commonly approximated with mathematical functions containing two parameters, absolute magnitude *H* and slope factor *G* [11]. Alternatively, authors [12,10] introduced following equation to fit the asteroids phase functions:

$$V(1,\alpha) = H - \frac{a}{(1+\alpha)} + b \times \alpha \qquad (4)$$

where $V(1,\alpha)$ is brightness of object obtained under phase angle α, *a* is opposition effect amplitude, *b* is the parameter describing the linear part of the curve. For better visualization, example of phase function of asteroid 44 Nysa with strong opposition effect is shown in Fig. 4.

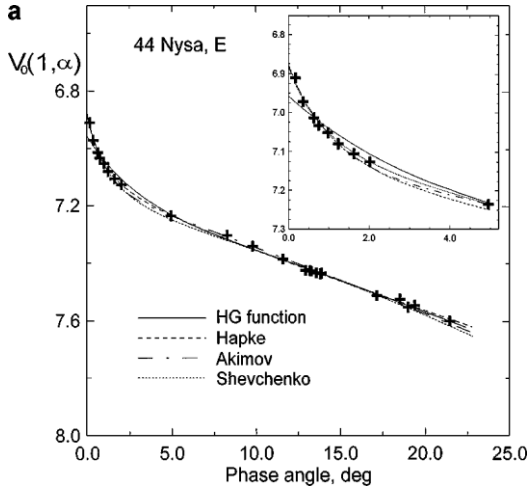

Figure 4. Fitted phase curve for 44 Nysa using various phase functions. Taken from [10]

2.4 Physical parameters

Previous sections introduced quantities which can be directly extracted from the measurements and can be used for object classification. However, to characterize the object, these quantities need to be transformed to values which represents physical properties of the object. There are two options how to proceed. In works [3,9] authors introduced equations which can be directly used to obtained physical parameters such as bond albedo ρ_b and/or mean cross section *C*:

$$V(1,\alpha) = -26.74 - 2.5log\big(C\rho_b * F_1(\alpha)\big) + 5log(R) \qquad (5)$$

where *R* is the distance between object and observer in Astronomical units [AU].

Other approach is used by minor planets community which has demonstrated that the measured quantities *H* and *b* (see Eq. 4) can be also used to extract the physical parameters. Commonly used relation between the absolute magnitude of the object and its diameter *D* assuming homogenous sphere is [13]:

$$log_{10}(D) = 3.1236 - 0.2H - 0.5log_{10}(\rho_v) \qquad (6)$$

Work of [12,10] based on observations of IRAS (Infrared Astronomical Satellite) Minor Planet Survey, which provided geometric albedos for minor planets of different types, found linear dependency between measured albedos ρ_v and slope parameter *b* (see Eq. 4):

$$b = 0.013(\pm 0.002) - 0.024(\pm 0.002)log_{10}(\rho_v) \qquad (7)$$

Eq. 7 demonstrates, that for some populations, in this case different asteroid families, there is link between the slope parameter *b*, which can be directly obtained from measurements along with parameter *H*, and the object's physical property ρ_v. We are not stating this relation is applicable to the artificial debris object, rather than we are demonstrating that there is a physical meaning behind the slope parameter *b*.

3 INSTRUMENTATION AND DATABASES

Within this work we are using data from two different sources, Space Debris Light Curve Database and Mini-Mega-TORTORA database, discussed further in next sections.

3.1 Space Debris Light Curve Database

The Space debris Light Curve Database (SDLCD) is database of the Faculty of Mathematics, Physics and Informatics, Comenius University in Bratislava (FMPI) and contains processed data observed on Astronomical and geophysical observatory in Modra [5]. The main catalogued objects are on geosynchronous, eccentric, global navigation satellite system orbits with recent extension toward Low-Earth Orbits (LEO) [14].

The main instrument for the space debris photometric data collection which provided light curves to SDLCD is FMPI's Newtonian design telescope AGO70 with a very thin 700 mm parabolic mirror from Alluna optics supported by gravity actuator. The focal length of the system is 2962.0 mm. The light from the telescope is detected by the CCD camera FLI-ProLine KAF-1001E Grade 1 front-illuminated full frame monochrome CCD Camera with 65 mm shutter and the resolution of 1024x1024 pixels with pixel size 24 mm. The resulting effective field of view is 29.1'x29.1' and pixel's field of view is 1.67"x1.67".

SDLCD contains (to date April 2020) in total 543 tracks (light curves) for 356 individual objects. All tracks are in arbitrary instrumental magnitude system and are not reduces to standard system. From 543 tracks, 512

showed periodic signal and the apparent rotation period could be extracted and the rotation phase could be constructed for them. Example of such rotation phase can be seen in Fig. 2.

For more about SDLCD and its data can be found in [5].

3.2 Mini-Mega-TORTORA database

Mini Mega Tortora (MMT) is wide-field monitoring system with nine channels for optical observations of the sky, mounted in pairs on five stands and is operated by Special Astrophysical Observatory of Russian Academy of Sciences, Russia. The research and observations are focused on detecting meteor events, satellites tracking and multi-color data of celestial bodies. The system is placed in Caucasus, with ability to detect objects with brightness level up to 10 magnitude. The used exposition time is 0.1 second. After the observation a light curve is constructed, processed and published in online MMT catalogue [15,16].

Every track in the catalogue contains: light curves in standard and apparent magnitudes, distance, phase angle over time, light curve period, whether the object was in penumbra, etc. Only 20% of all tracks are periodical. All objects are divided into type groups: active spacecrafts, non-functioning spacecrafts, spacecrafts without specification of the functional state, rocket bodies, operational fragments of launch, fragments of destruction, fragments without specification of the method of formation of unknown types. Database does not contain measurement errors and data of Russian objects, which are only available on request. The MMT database contains 3662 objects, from which 1366 (37.3%) are slow rotators, 1388 (37.9%) are stable and 908 (24.8%) are rotators.

In Fig. 5 is plotted comparison between two reference databases, SDLCD and MMT, namely apogee vs perigee altitudes of catalogued objects.

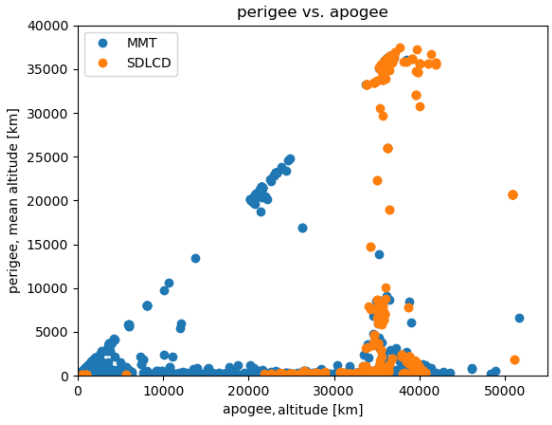

Figure 5. Orbital elements of objects catalogued by MMT (blue) and SDLCD (orange) database. To April 2020. Source: SDLCD [5] and MMT [16]

4 SPACE OBJECTS CLASSIFICATION

First parameters which can be immediately extracted once the rotation phase is fitted as described in Section 2.1 are signal amplitude A and complexity X. Because there is no need to be in standard system to perform this step, this has been done for 512 light curves obtained in SDLCD (see Section 3.1). In Fig. 6 and Fig. 7 are plotted histograms of calculated amplitudes A and complexities X for 164 upper stages (R/B) and 71 payloads (P/L) present in the SDLCD in April 2020.

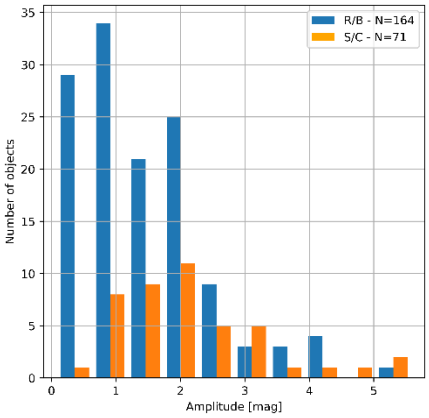

Figure 6. Amplitudes extracted from rotation phases obtained from 235 light curves for 164 R/Bs and 71 P/Ls. Source: SDLCD [6]

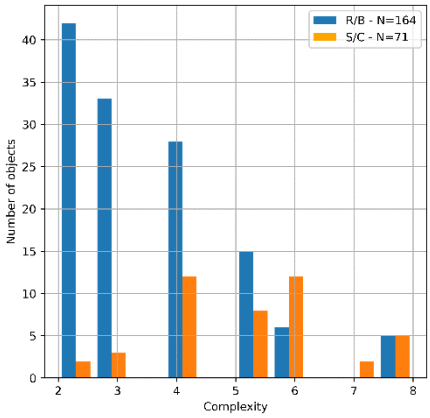

Figure 7. Complexities extracted from rotation phases obtained from 235 light curves for 164 R/Bs and 71 P/Ls. Source: SDLCD [6]

By investigating dependency X vs A, we can see some characteristic values for selected populations as plotted in Fig. 8. While for Atlas 5 Centaur R/B the maximum amplitude reached value of A_{max} = 5.5 mag, its complexity is most cases X_{max} = 2 (marked by blue cross). SL-12 R/B population shows simple complexity of X_{max} = 2 with relatively small A_{max} = 2.5 mag. Raduga P/L population is very complex with X_{max} = 6 and A_{max} = 3.2 mag.

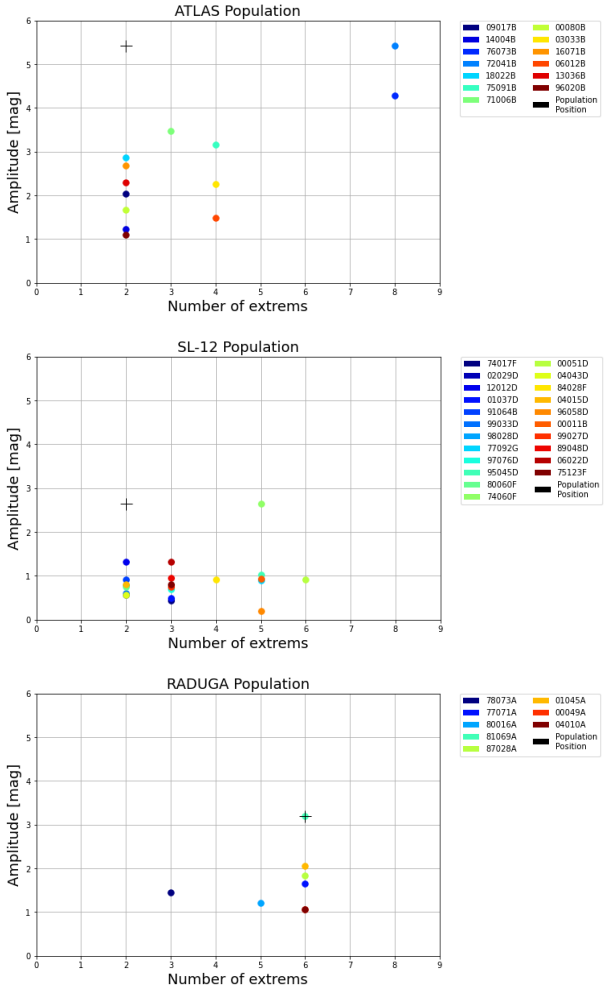

Figure 8. Number of extrema (maxima or minima) vs amplitude extracted from rotation phases of three different populations, Atlas 5 Centaur R/B (upper figure), SL-12 R/B (middle figure) and Raduga P/L (lower figure). Source: SDLCD [6].

When we plot obtained values for X_{max} vs A_{max} for different populations, we can start to see clusters. This is visible in Fig. 9 where are plotted quantities for populations most often present in SDLCD database.

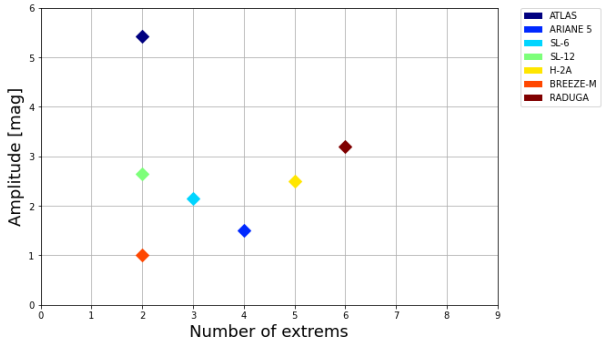

Figure 9. Representative values for number of extrema (maxima or minima) vs maximum amplitude for given population. Source: SDLCD [6].

5 SPACE OBJECTS CHARCERIZATION

For object characterization we used MMT database which covers wide range of phase angles for relatively large number of objects.

5.1 Simple shaped objects

First, we focused on calibration targets, such as radar calibration spheres, to validate the data, as well the theory behind the processing. From MMT extracted could be data for specular calibration sphere LCS 1 (65034C, 1361) and diffuse white calibration sphere Calsphere 4 (65065H, 1520). While LCS 1 was fitted with phase function for specular sphere (Eq. 3), Calsphere 4A was fitted with phase function for diffuse sphere. Extracted data (blue points), as well the fitted curves (red line), can be seen in Fig. 10 and Fig. 11. Blue measurement points have been calculated by using average value of measurement points within 3° interval of phase angle.

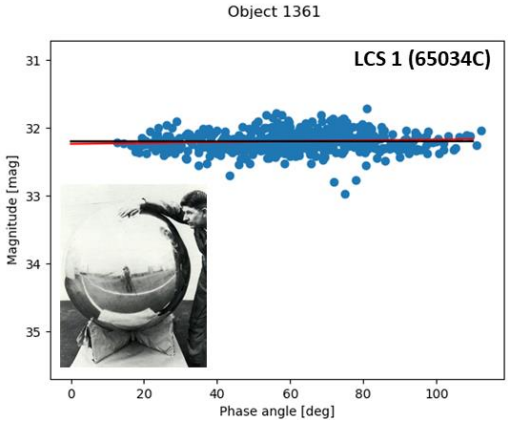

Figure 10. Phase function of LCS 1 (65034C, 1361). Data source: MMT database [16], Photo credit: [17].

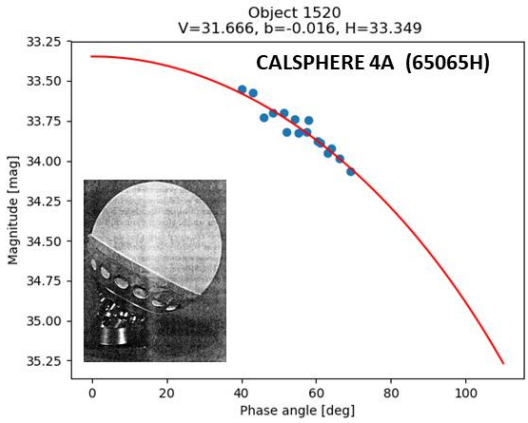

Figure 11. Phase function of Calsphere 4 (65065H, 1520). Data source: MMT database [16], Photo credit: [17].

By fitting the phase functions, we could extract the absolute magnitudes for both spheres, which were H = 32.1 mag and H = 33.349 mag, respectively. Diameter of both spheres is according to the public sources 1.12 m. This would mean that the geometric albedo ρ_v according to Eq. 6 would be 0.15 (assuming diffuse source) and 0.05, respectively. By comparing these values to values reported by [3] 0.59 and 0.67, we see discrepancy. This will be further investigated.

5.2 Cylindrical objects

Another step was to investigate the measured quantities for cylindrical shaped objects for which the data are present in the MMT database. Before we moved to the processing, it was necessary to select the proper phase function which would be the best to represent the measured data and populations. By looking at the functions commonly used in asteroid community discussed in Section 2.3, we shall expect linear behavior, as well incorporate the opposition effect. However, for geocentric objects, which are in close vicinity of the Earth (closer than 40,000 km), this effect can't be observed by ground-based telescopes as demonstrated in Fig. 12. Plotted is histogram of around 35 million MMT measurement points.

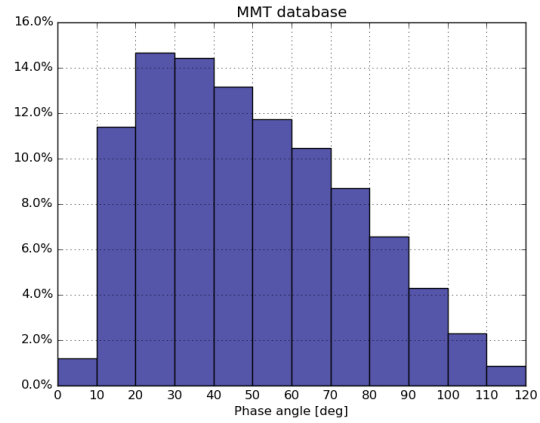

Figure 12. Phase angles covered by MMT system. Data compiled from around 35 million photometric measurement points. Data source: MMT database [16].

Histogram in Fig. 12 clearly demonstrates that it is highly unlikely to obtain brightness information for small phase angles ($\alpha < 5°$) from which the opposition effect can be assessed. This means that by applying phase functions from asteroid community to such data sets would lead to miss-leading results. On the other side, it is preferable to still describe the debris phase function with two components, linear for large phase angles and another one to describe small phase angles.

It is assumed that space debris objects would contain diffuse, as well specular component. However, we assume that for simple shaped objects such as upper stages, assumption of phase function for diffuse sphere should be sufficient for initial analysis. We decided to modify the Eq. 4, where we replaced the coefficient a with phase function for diffuse sphere (Eq. 2):

$$V(1,\alpha) = H - log_{10}\big(F_1(\alpha)\big) + b \times \alpha \qquad (8)$$

We applied Eq. 8 to few selected cases with good data representation within MMT database. Phase functions for four selected cases can be seen in Fig. 13 – 16. To obtain the blue measurement points, we constructed rotation phase data sets within each 3° size interval and from each rotation phase we used parameter a_0 from Eq. 1 as the measurement point (blue points) to be fitted with phase function defined in Eq. 8. (red line).

In Fig. 13 is plotted phase function for Atlas 5 Centaur R/B for which we extracted H = 23.756 mag and b = 2.394. This object would have diameter of 56 m assuming geometric albedo of 0.175 [18]. In Fig. 14 is plotted phase function for H-2A R/B for which we extracted H = 23.716 mag and b = 0.6. This object would have diameter of 57 m assuming geometric albedo of 0.175. In Fig. 15 and Fig. 16 are plotted phase functions for CZ-3B R/Bs for which we extracted H = 22.6 mag and H = 22.228 mag and b = 2.562 and b = 1.209, respectively. These objects would have diameter of 96 m and 110 m.

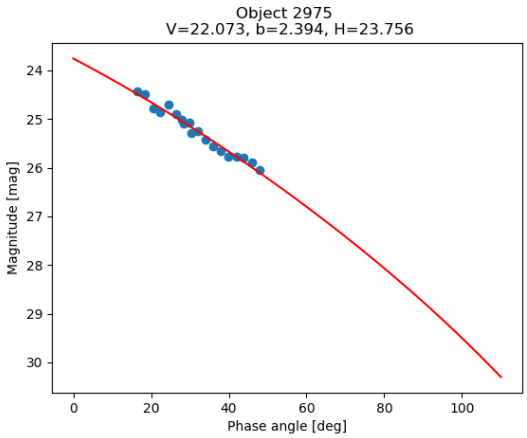

Figure 13. Phase function of Atlas 5 Centaur R/B. Data source: MMT database [16].

6 CONCLUSIONS

Parameters extractable from photometric measurements allow to perform object classification and characterization. Light curves, namely the ones acquired for rotating objects, can provide the information about the object's complex shape and dimensions. By performing longer series, additional parameters related to size and albedo can be extracted, parameters such as absolute magnitude and slope factor.

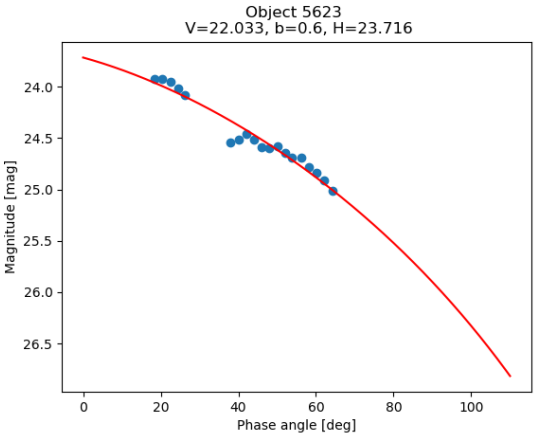

Figure 14. Phase function of H-2A R/B (17062B, 42966). Data source: MMT database [16].

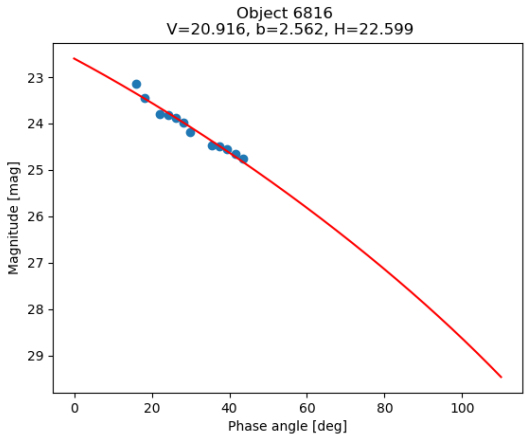

Figure 15. Phase function of CZ-3B (19090D, 44867). Data source: MMT database [16].

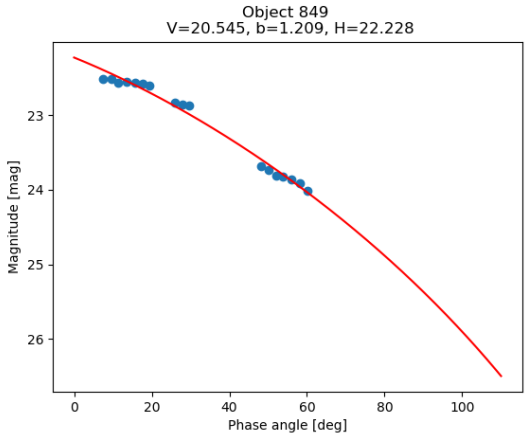

Figure 16. Phase function of CZ-3B (13075B, 39482). Data source: MMT database [16].

In our work we presented phase functions commonly used in astronomical and debris communities and we proposed our own function to be applied to debris photometric measurements as a first assumption. We presented methodology how such functions can be applied to extensive data sets which are currently publicly available via databases like Mini-MegaTORTORA (MMT) catalogue and Comenius University's Space Debris Light Curve Database (SDLCD).

We analyzed several test cases for which we extracted data from MMT database and for which we can assumed simple shapes such as sphere or cylinder. Our initial assessment showed that absolute magnitude and slope parameter can be close to realistic values but more analysis on much wider data sets needs to be performed.

Analysis of rotation phases of different populations revealed clustering in parameter space defined via complexity (number of extrema in rotation phase) and maximum measured amplitude.

In our next work, we will focus on applying the defined phase function to large amount of objects present in the MMT database. We expect to extract parameters such as absolute magnitude, slope parameter, maximum amplitude and complexity for more than 500 objects, while we will be focusing on definition of classification of populations according to these parameters, as well to extract physical quantities for known populations, e.g., geometric albedo.

SDLCD will be improved by transforming photometric points into standard system. This database will be used to analyze parameters of fragmentation debris objects situated on orbits with mean altitudes higher than 10,000 km and for which smaller phase angles can be reached comparing to MMT. SDLCD data will be also used for cross-check analysis of MMT data.

7 REFERENCES

1. Fan, S., Frueh, C., A Direct Light Curve Inversion Scheme and the Influence of Measurement Noise, Journal of Astronautical Science, submitted 2018.

2. Zigo, M., Žilková, D., Šilha, J., Matlovič, P., Tóth, J., Combined effort of reflectance spectroscopy and BVRI photometry in the field of space debris characterization, Proceedings of the 8th European Conference on Space Debris, Darmstadt, Germany, 2021.

3. Africano, J., Kervin, P., Hall, D., Sydney, P., Ross, J., Payne, T., Understanding Photometric Phase Angle Corrections, Proceedings of the 4th European Conference on Space Debris (ESA SP-587). 18-20 April 2005, ESA/ESOC, Darmstadt, Germany. Editor: D. Danesy., p.141.

4. Schildknecht, T., Musci, R., Ploner, M., Beutler, G., Flury, W., Kuusela, J., de Leon Cruz, J., de Fatima Dominguez Palmero, L., 2004. Optical observations

of space debris in geo and in highly-eccentric orbits. Adv. Space Res. 34, 901–911. http://www.sciencedirect.com/science/article/ pii/S0273117704000651, doi:https://doi.org/10.1016/j.asr.2003.01.009.

5. Silha J., S. Krajcovic, M. Zigo, J. Toth, D. Zilkova, J. Vilagi, P. Zigo, L. Kornos, J. Simon, T. Schildknecht, E. Cordelli, A. Vananti, H. Mann, A. Rachman, Paccola Ch., and T. Flohrer. Space debris observations with the slovak AGO70 telescope: astrometry and light curves. Advances in Space Research, 2020.

6. Scargle, J.D., 1982. Studies in astronomical time series analysis. ii – statistical aspects of spectral analysis of unevenly spaced data. Astrophys. J. 263, 835–853. https://doi.org/10.1086/160554, http:// adsabs.harvard.edu/abs/1982ApJ...263.835S.

7. Schwarzenberg-Czerny, A., 1997. The correct probability distribution for the phase dispersion minimization periodogram. Astrophys. J. 489, 941–945. https://doi.org/10.1086/304832, http://adsabs.harvard.edu/abs/1997ApJ...489.941S.

8. Pravec, P., Harris, A., Scheirich, P., Kusniraak, P., Sarounova, L., Hergenrother, C., Mottola, S., Hicks, M., Masi, G., Krugly, Y., Shevchenko, V., Nolan, M., Howell, E., Kaasalainen, M., Gala´d, A., Brown, P., DeGraff, D., Lambert, J., Cooney, W., Foglia, S., 2005. Tumbling asteroids. Icarus 173, 108–131. http://www.sciencedirect. com/science/article/pii/S0019103504002568, doi:https://doi.org/ 10.1016/j.icarus.2004.07.021. hapke Symposium.

9. Hejduk, M., Specular and Diffuse Components in Spherical Satellite Photometric Modeling, Proceedings of the Advanced Maui Optical and Space Surveillance Technologies Conference, held in Wailea, Maui, Hawaii, September 13-16, 2011, Edited by S. Ryan, The Maui Economic Development Board, 2011., id.E15.

10. Belskaya, I.N., Shevchenko, V.G., Opposition Effect of Asteroids, Icarus, Volume 147, Issue 1, September 2000, Pages 94-105, DOI:10.1006/icar.2000.6410.

11. Bowell, E., Hapke, B., Domingue, D., Lumme, K., Peltoniemi, J., Harris, A. W., Application of photometric models to asteroids, Asteroids II; Proceedings of the Conference, Tucson, AZ, Mar. 8-11, 1988 (A90-27001 10-91). Tucson, AZ, University of Arizona Press, 1989, p. 524-556.

12. Shevchenko, V. G., Analysis of the Asteroid Phase Dependences of Brightness, Lunar and Planetary Science, volume 27, page 1193, 1996.

13. Muinonen, K., Belskaya, I., Cellino, A., Delbo, M., Levasseur-Regourd, A.-Ch.,. PenttilÃ, A., Tedesco, Ed., A Three-Parameter Magnitude Phase Function for Asteroids, Icarus. 209. 542-555, 10.1016/j.icarus.2010.04.003, 2010.

14. Šilha, J., Krajcovic, S., Zigo, P., Toth, J., Zigo, M., Žilková, D., Jilete, B., Flohrer, T., Development and operational status of AGO70 telescope, Proceedings of the 8th European Conference on Space Debris, Darmstadt, Germany, 2021.

15. Karpov, S., Massive photometry of low-altitude artificial satellites on Mini-Mega-TORTORA, IV Workshop on Robotic Autonomous Observatories, Revista Mexicana de Astronomía y Astrofísica (Serie de Conferencias) Vol. 48, pp. 112-113, 2016.

16. MMT: Satellites identified in MMT data: April 27, 2020, available at: http://mmt9.ru/satellites/

17. Gunter's Space Page, March, 2021, available at: http://space.skyrocket.de

18. Mulrooney, M., Matney, M., Barker, E., “A New Bond Albedo for Performing Orbital Debris Brightness to Size Transformations.” 2008 International Astronautical Congress, Glasgow, Scottland, October 2008.